Hindawi
Advances in Civil Engineering
Volume 2020, Article ID 9198356, 10 pages
https://doi.org/10.1155/2020/9198356

Research Article

A Modified Cubic Law for Rough-Walled Marble Fracture by Embedding Peak Density

Baohua Guo,[1] **Chenlin Wang**,[1] **Long Wang**,[2] **Yan Chen**,[1] **and Tan Cheng**[1]

[1]*School of Energy Science and Engineering, Henan Polytechnic University, Jiaozuo, Henan 454000, China*
[2]*School of Safety Science and Engineering, Henan Polytechnic University, Jiaozuo, Henan 454000, China*

Correspondence should be addressed to Long Wang; 18336860596@163.com

Received 5 April 2019; Revised 4 September 2019; Accepted 1 November 2019; Published 3 January 2020

Academic Editor: Timo Saksala

The property of water flow through a single rock fracture is the base of describing the seepage characteristics of jointed rock mass. Five artificial tensile fractures of coarse-grained cylinder marble samples were made at about the midpoint of the long axis by using a self-made splitting mold. The upper and lower surfaces of the tensile fractures were scanned by a 3D laser scanner (OKIO) to obtain their 3D coordinates. Then, the Geomagic Studio Software and rock surface topography scan test software were used to obtain peak density values of each single fracture surface. To study the seepage characteristics of open fracture, 4 rectangular plastic spacers with the size of about 3 mm × 2 mm × 0.2 mm were put into the fracture when water flowed through the single rough fracture tests were conducted under different normal stresses using the self-developed radial flow system. According to the testing data, the relationships between the seepage characteristics of single rough rock fracture and the peak density of fracture surface were studied. It is discovered that the 3D fracture morphology had great influences on the seepage characteristics of the single rock fracture. A modified cubic law was put forward to present the relationship between the seepage characteristics of a rough rock fracture and peak density of two fracture surfaces. Comparison between the modified cubic law and the experimental data showed a relatively good agreement.

1. Introduction

Groundwater flow through jointed rock mass affects the stability of many engineering structures in civil engineering, mining engineering, hydropower engineering, petroleum engineering, and environmental engineering [1]. The water flow through a single rock fracture is usually the base of describing the seepage characteristics of jointed rock mass, which is why the water flow through a single rock fracture has been tested extensively in laboratory by a number of researchers.

In the early research on the seepage model for water flow through a single fracture, Lomize [2], De Marsily and Romm [1, 3], and Louis [4] firstly carried out the water flow test through two parallel plates and developed the so-called cubic law, which stated that the flow rate through the parallel plates had a cubic relation with the aperture of the plates. Thus, tiny change of the aperture may lead to major variation of the seepage flow rate. However, the surface of natural fractures is usually rough and undulant instead of smooth. If the aperture is large enough, the effect of rough and undulant fracture surface on the seepage characteristics of rock fractures may be slight [5] or negligibly low [6]. Singh et al. [7] found that water flowing through a single rough fracture in granite still obeyed the well-known "cubic law" even if the fractures were under the combination conditions of high b_p (maximum inlet water pressure, 25 MPa) and σ_3 (maximum confining pressure, 40 MPa). However, Konzuk and Kueper [8] summarized the research progress achieved on the seepage properties of rough rock joints and modified cubic law and suggested that the applicability of the local cubic law should be studied under the condition of different fracture surface three-dimensional morphology or/and abrupt aperture changes. Moreover, Raven and Gale [9] found the deviation of the relationship between the joint flow rate and the joint deformation from behaviour predicted by the

parallel plate model increased with the sample size and the number of loading cycles increasing. Therefore, the validity of the cubic law is suspicious [10, 11], and the cubic law has a certain limitation in practical application.

Correspondingly, in order to still apply the cubic law in analyzing seepage properties of rough rock fracture, various researchers have tried to modify the cubic law by incorporating some fracture roughness parameters. JRC (joint roughness coefficient) is usually used to describe rock joint roughness in rock engineering since the morphology of the actual rock joint is usually very complex and it is difficult to completely describe the profile feature of the rock joint according to the 10 standard section lines [12]. Jaeger et al. [6, 10, 11] studied the effect of rock joint roughness on the seepage properties of the joint from different point of views and modified the cubic law by using JRC to quantify the rock joint roughness so that the modified cubic law could be applied in analyzing the seepage characteristics of the rough rock joint. Neuzil [13] and Park and Hahn [14] imported a function of aperture density distribution to analyze the effect of joint surface roughness on the joint seepage properties. Iwai [15] conducted the seepage experiment and concluded that the way of the joint roughness affecting on the water flow through a single joint was related to the contact ratio of the rock joint surfaces. Subsequently, Zhou and Xiong [16] put forward a modified cubic law by incorporating a joint contact ratio. Zhao [17] proposed a new parameter, i.e., JMC (joint matching coefficient), to describe the effect of the contact state on the seepage characteristics of the rock joint qualitatively. Tsang and Tsang [18] proposed a channel model to describe the seepage property of the rock joint based on the integrated laboratory test and theoretical analysis. Luis et al. [19] studied the channel flow phenomenon of seepage and solute transport in a single joint using the discrete element method. Brown et al. [20] studied the effect of joint roughness on the joint seepage properties using the Reynolds equation and the fractal model of joint surface morphology. A friction factor was introduced in reference [21] as a function of two-independent variables, Reynolds number and relative roughness, and was then formulated to describe the influence of friction drag of the wall and local aperture changes on pressure head distribution.

Since the fracture surface is rough, the cubic law with the use of average aperture may not be able to describe the true seepage characteristics of the rough rock fracture. Moreover, as reviewed above, most of the modified cubic laws have used either JRC or the fracture aperture distribution function to characterize the influence of the fracture roughness on the fracture seepage properties although neither JRC nor the aperture distribution function are easy to obtain. Therefore, the objective of this paper is to put forward a modified cubic law to present the relationships between the seepage characteristics and a 3D fracture morphology parameter of a rough fracture by conducting water flow tests through a single rough fracture.

2. Materials and Methods

2.1. Sample Preparation. Five cylindrical samples with a diameter of 50 mm and a height of 100 mm were firstly manufactured from white coarse-grained marble, then a blind hole with a length of 60 mm and a diameter of 6 mm was drilled from one end along the axis of each cylindrical sample; finally, a self-designed splitting mold, as shown in Figure 1(a), was used to divide each cylinder sample into two halves at about the midpoint of the long axis. The splitting mold consists of two identical parts, each of which consists of an iron plate with a cylindrical groove and a wire with a triangular cross section. The iron plate has a slot at the midpoint of the long axis perpendicular to the axis and the wire is fixed in the slot to split the sample with an edge. Marble fracture surfaces of sample M1 and 5 single-fractured samples are shown in Figure 1(b).

2.2. 3D Morphology Parameters of Rock Fracture Surface. The upper and lower surfaces of the tensile fractures in a coarse-grained marble were firstly scanned by a Tianyuan OKIO-typed 3D laser scanner with CCD camera resolution of 1.44×106 pixel and with measurement accuracy of up to 10 μm, as shown in Figure 1(c), and the distance between adjacent points was about 16 μm. Marking points (black rings on the surface of the sample, as shown in Figure 1(b)) are used to control the stitching of scanning data because one time of scan is incomplete to obtain all the morphological data of a fracture surface. The coordinates of the scanned surface will be written in ASCII or binary files in the X, Y, and Z format, in which X, Y, and Z coordinates represent the width, length, and height of the fracture surface, respectively. Subsequently, the ASCII or binary files were imported to the Geomagic Studio Software to complete the encapsulation of the sample surface and were saved as OBJ files, and encapsulated fracture surfaces of the sample M1 were illustrated in Figures 1(d) and 1(e), respectively. Finally, the OBJ files were imported to Rock Surface Topography Scan Test Software (RSTST) by which 3D fracture morphology parameters could be calculated. In the scanned point cloud grid network, the point on the fracture surface is selected as a peak if its height is higher than its adjacent eight points. Peak density S_{pd} is the peak number in the unit area, and it can be obtained by the number of all the peak points being divided by the projected area of fracture surface, as shown in Table 1.

2.3. Flowing Test Device. Figure 2(a) depicts the test system for studying the seepage characteristics of the splitting fracture, which includes three parts, i.e., the water supplying system, the loading-seepage-measurement system, and the water collecting system. The inlet water head is controlled by the height of the water tank relative to the position of the rock fracture. The loading-seepage-measurement system includes normal loading system, normal deformation measurement system, and water switch. The water collecting system mainly includes heat-shrink tubing (collecting water outflow from the rock fracture), discharging tube, beaker, and balance. The upper and lower parts of heat-shrink tubing were tightened by the pipe clamp after their shrinkage by heating, and the middle part of the heat-shrinkable tubing near the fracture plane outlet had no pressure on the sample

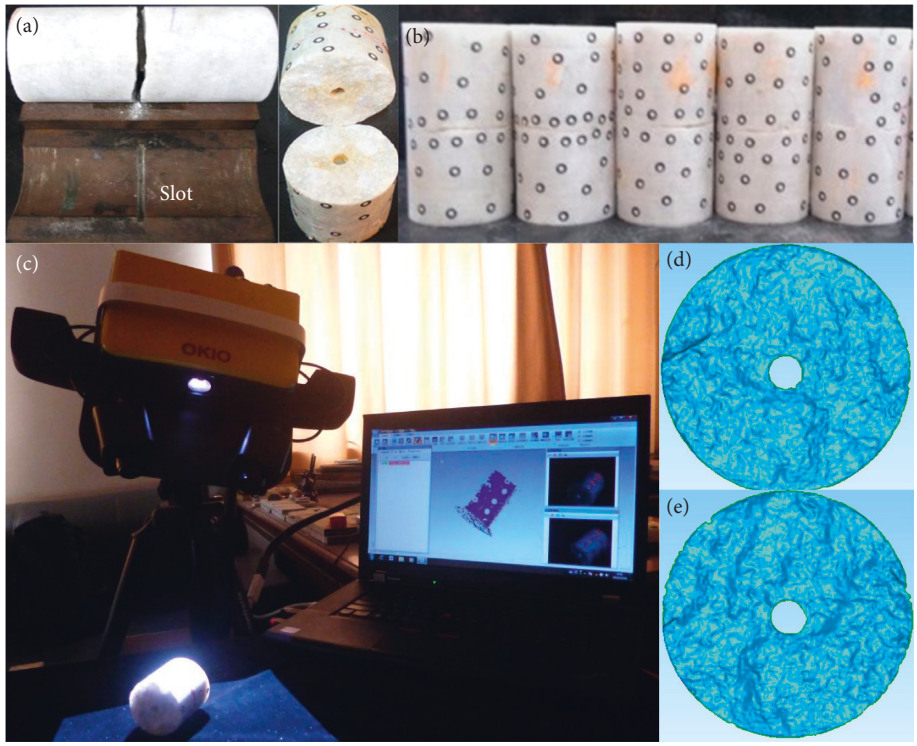

Figure 1: Test device and preparation of samples. (a) Self-made splitting mold; (b) marble fracture surfaces and single-fractured samples; (c) 3D laser scanning device; (d) 3D morphology of sample M1 upper fracture; (e) 3D morphology of sample M1 lower fracture.

Table 1: S_{dp} of five rock fractures (cm^{-2}).

	M1	M2	M3	M4	M5
Upper fracture	0.64	0.32	0.40	0.07	0.32
Lower fracture	0.06	0.33	0.26	0.51	0.38
Maximum	0.64	0.33	0.40	0.51	0.38
Average	0.35	0.32	0.33	0.29	0.35
Minimum	0.06	0.32	0.26	0.07	0.32

side. Vaseline was filled between the heat-shrinkable tube and the side surface of the sample within the specified range of the two pipe clamps to prevent water from flowing out through the upper or lower part of the heat-shrinkable tube.

The normal load is applied on the sample through a self-developed creep testing device UCT-2, which includes upper pressure head, lower pressure head, and feed water plate, as shown in Figure 2(a). The normal stress can then be calculated according to the pump pressure and the cross-sectional area of the rock sample. The normal displacement is measured by three equidistant dial indicators attached to the rods which are fixed to the upper plate. The measuring heads of the three dial indicators touch the ring plate which is fixed to the sample. Thus, the reading variation of the three dial indicators can reflect the normal displacement between the upper plate and the ring plate, the average of which is taken as the normal deformation of the rock fracture approximately under lower normal stress levels.

2.4. Test Procedure. The single-fractured specimen in the radial flow test is shown in Figure 2(b). Four rectangular plastic spacers with the size of about 3 mm × 2 mm × 0.2 mm were placed in the fracture to make sure the fracture remains open and their size was very small compared with that of the fracture so that the four rectangular plastic spacers had little effect on the water seepage through the fracture. During the radial flow test, the water was supplied from the inlet hole and then flowed along the blind hole reaching the rock fracture. After that the water seeped radially from the centre of the specimen through the rock fracture and finally left the fracture flowing into the breaker through the discharging tube. During the radial flow test, a constant normal stress was applied on the rock fracture, which was set as 1~6 MPa, respectively. Under each normal stress, the inflow water head were all set as 22 m. The readings of three dial indicators are recorded once normal stress or water head changed.

3. Results and Discussion

3.1. The Flow State of Fluid through a Rock Fracture. Reynolds number R_e can describe the flow state of fluid and reflect the influence of parameters such as flow velocity, viscous coefficient of fluid, and shape of seepage passage. By calculating Reynolds number, the flow state of water through a rock fracture can be judged. The calculation formula is as follows:

$$R_e = \frac{vL\rho}{\mu}, \quad (1)$$

where R_e is Reynolds number; v is characteristic velocity, m/s; μ is dynamic viscous coefficient of water; the temperature

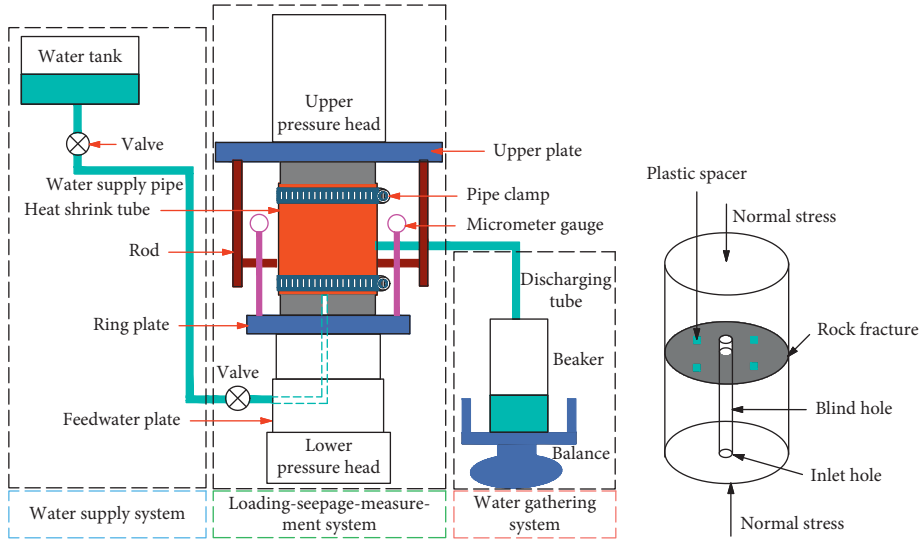

Figure 2: Schematic sketch of the (a) radial flow testing system and (b) specimen in test.

of water is about 10°C; $\nu = 1.31 \times 10^{-3}$ kpa·s; L is characteristic length, and for fracture flow, its value is twice the equivalent hydraulic aperture [22].

In the test, the seepage flow starts from the inner hole boundary of the sample and flows radially along the fracture surface to the outer circumference. The flow velocity and Reynolds number are different at the inner and outer boundary of the fracture surface. According to the test scheme, when the initial normal stress is 2 MPa and the head difference is 22 m, the flowrate and Reynolds number calculated are the largest. The inner Reynolds number R_{ei} and the outer Reynolds number R_{eo} are calculated as shown in Table 2. From Table 2, it can be seen that under initial normal stress of 2 MPa, the inner Reynolds number R_{ei} is greater than the outer Reynolds number R_{eo} and its maximum value is 9.54, which is far less than the critical Reynolds number 500. Therefore, the flow state of water through the rock fracture can be considered as laminar flow. In addition, the permeability of intact rock is generally very small and its permeability coefficient is generally less than 10^{-7} cm/s. The minimum rock fracture permeability coefficient in this paper is 5.38×10^{-3} cm/s, which is about 4 orders higher than that of intact rock; thus, the influence of rock permeability on rock fracture seepage test results can be neglected.

3.2. The Basic Theory of Radial Flow in a Single Fracture. The cubic law was derived from the Navier–Stocks equation based on the smooth parallel plates model as follows:

$$\mu = -KJ, \tag{2}$$

$$K = \frac{g}{12\nu} b^2, \tag{3}$$

where μ is flow velocity, K is hydraulic conductivity, J is hydraulic gradient, ν is kinematic viscosity coefficient, g is acceleration of gravity, and b is mechanical aperture.

Table 2: Initial Reynolds number.

Sample	M1	M2	M3	M4	M5
R_{ei}	4.16	8.43	9.71	9.16	9.54
R_{eo}	0.5	1.01	1.17	1.1	1.14

$\nu = 1.31 \times 10^{-6}$ kpa·s at room temperature of 10°C and $g = 9.8 \times 10^3$ kg/m^3.

Based on the seepage theory for groundwater flow, the radial flow rate can be calculated using the following equation:

$$Q = -K \frac{dH}{dr} 2\pi r b, \tag{4}$$

where Q is flow rate, r is radius, and H is water head.

Equation (4) can be integrated to become

$$\frac{Q}{\Delta H} = \frac{2\pi}{\ln(R/r_0)} Kb, \tag{5}$$

where R is the outer boundary radius, r_0 is the internal boundary radius, and ΔH is head difference.

Combining equation (3), equation (5) is written as

$$\frac{Q}{\Delta H} = \frac{\pi g}{6\nu In(R/r_0)} b^3. \tag{6}$$

Equation (6) can be simplified as follows:

$$\frac{Q}{\Delta H} = Cb^3, \tag{7}$$

where

$$C = \frac{\pi g}{6\nu In(R/r_0)}. \tag{8}$$

Equation (7) is used to describe the radial flow through smooth parallel plates. Since natural fractures are usually rough, equivalent hydraulic aperture b_e can be used to replace the aperture b in equation (7), that is,

$$\frac{Q}{\Delta H} = Cb_e^3. \quad (9)$$

3.3. The Relations between Equivalent Hydraulic Aperture and Fracture Closure. Fracture aperture directly affects the seepage flow, but it is difficult to measure the fracture aperture directly. On the other hand, the fracture closure can be easily measured. The fracture closure reaches the maximum value when the equivalent hydraulic aperture b_e calculated by equation (9) is zero theoretically. Figure 3 shows the relationship between the equivalent hydraulic aperture b_e and fracture closure Δb obtained from the water radial seepage through the fractures of 5 specimens under six normal stresses described in Section 2.

It can be seen from Figure 3 that the equivalent hydraulic aperture b_e decreases linearly with the fracture closure Δb increasing as a whole. That is, the equivalent hydraulic aperture b_e has a negative linear correlation with the fracture closure Δb. Thus, when the equivalent hydraulic aperture b_e decreases and reaches zero, the maximum mechanical aperture $(b_m)_{max}$ which is defined as the maximum normal closure Δb of the rock fracture can be obtained. Therefore, the mechanical aperture b_m under different normal stresses can be calculated by subtracting normal closure Δb from maximum mechanical aperture $(b_m)_{max}$. The relationship between the equivalent hydraulic aperture and the fracture closure is

$$b_e = p_1 \Delta b + p_2, \quad (10)$$

where p_1 and p_2 are fitting parameters.

3.4. The Relationship between the Flow Rate Per Head and Mechanical Aperture. Figure 4 depicts the relationship between the flow rate per head and the mechanical aperture obtained from the water radial seepage through the fractures of 5 specimens tests under different normal stresses. As can be seen from Figure 4, the flow rate per head increases with the mechanical aperture increasing, which can be well fitted by the power function in the following equation:

$$\frac{Q}{\Delta H} = p_3 b_m^n, \quad (11)$$

where p_3 is a fitting parameter and n is the exponent.

The values of p_3 and n and correlation coefficient R^2 are listed in Table 3 for the five fractures tested in the radial seepage tests. The correlation coefficients R^2 for all five fractures are above 0.94. The range of the exponent n is 2.94~3.17, i.e., close to 3, which is consistent with the general cubic relationship between the flow rate per head and the mechanical aperture. As the mechanical aperture increases, the increasing rate of the flow rate per head increases gradually. It is because the contact area between the fracture surfaces becomes larger and larger as the normal closure increases, which results in fewer flow paths and smaller flow rates. The fitting parameter p_3 in equation (11) reveals the influence of the fracture roughness on the flow rate, which is unequal to the coefficient C in equation (9) derived according to the smooth parallel plate model. Correspondingly, a correction coefficient ξ (Table 3) is introduced to modify equation (9), which becomes

$$\frac{Q}{\Delta H} = C\xi b_m^3. \quad (12)$$

After that, the relationships between the flow rate per head and the mechanical aperture are fitted again using equation (12) with the regression parameter ξ and correlation coefficients R^2 are listed in Table 3. As can be seen from Table 3, the correlation coefficients R^2 are all above 0.91.

Further, the relationship between the regression parameter ξ and the average peak density is shown in Figure 5. As can be seen from Figure 5, there is a power relationship between ξ and the average peak density $(S_{pd})_{ave}$ (which is one of the 3D morphology parameters), and the correlation coefficient is 0.91.

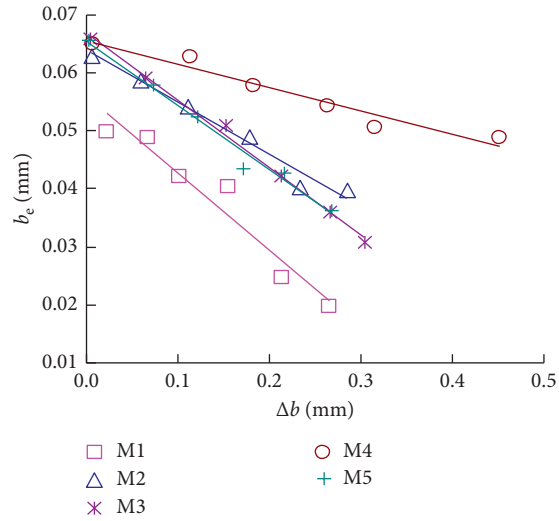

Figure 3: Relationships between equivalent hydraulic aperture and fracture closure.

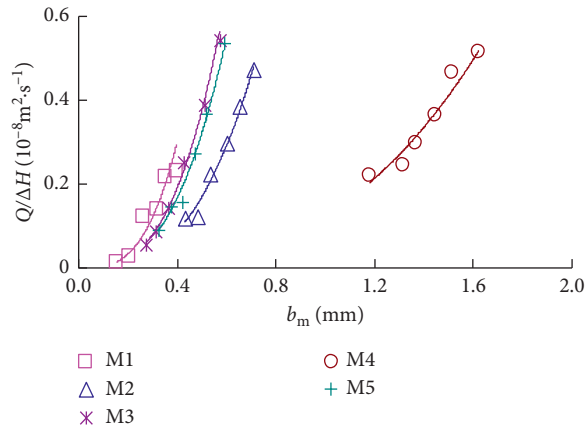

Figure 4: Relationships between flow rate per head and mechanical aperture.

Table 3: Fitting parameters and correlation coefficients R^2.

No.	$(b_e)_{max}$ (mm)	Equation (10)			Equation (11)			Equation (12)		Equation (14)		
		P_1	P_2	R^2	P_3	n	R^2	ξ	R^2	P_4	P_5	R^2
M1	0.45	−0.13	0.06	0.94	5.53	3.17	0.95	2.29	0.91	−0.05	0.45	0.99
M2	0.71	−0.09	0.06	0.98	1.34	2.98	0.97	0.72	0.99	−0.06	0.77	1.00
M3	0.58	−0.12	0.07	1.00	3.11	3.04	1.00	1.57	1.00	−0.06	0.63	0.99
M4	1.63	−0.04	0.07	0.95	0.13	2.94	0.94	0.07	0.95	−0.08	1.70	0.99
M5	0.59	−0.11	0.07	0.98	2.50	2.95	0.98	1.39	1.00	−0.05	0.63	1.00

If the fitting equation between ξ and the average peak density $(S_{pd})_{ave}$ illustrated in Figure 5 is substituted into equation (12), the following equation can be obtained:

$$\frac{Q}{\Delta H} = C \times 10^8 \left(S_{pd}\right)_{ave}^{16.83} b_m^3. \tag{13}$$

Equation (13) indicates that the relationship between the flow rate per head and the mechanical aperture is a modified cubic law containing the 3D morphology parameter S_{pd}. It should be pointed out that whether the proposed modified cubic law here can be used for a different rock fracture size needs a further study.

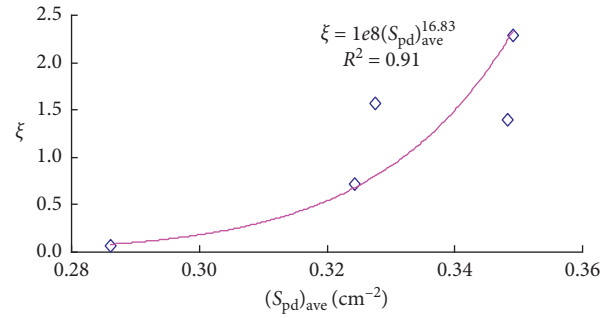

Figure 5: Relationship between ξ and $(S_{pd})_{ave}$.

3.5. The Relationship between Mechanical Aperture and Normal Stress. However, as mentioned before, the mechanical aperture is a parameter which cannot be easily obtained, but it is easy to obtain the normal stress during the fracture seepage test. Therefore, it is rather useful to build a relationship between the flow rate and the normal stress from the practical point of view.

Figure 6 depicts the relationship between the mechanical aperture and the normal stress obtained from the fracture seepage tests. As shown in Figure 6, the mechanical aperture decreases linearly with the increase of the normal stress and the decreasing rates are rather similar for all five specimens. Thus, the linear relationship between the mechanical aperture and the normal stress σ can be denoted using the following equation:

$$b_m = p_4\sigma + p_5, \tag{14}$$

where p_4 and p_5 are linear regression parameters.

The regression parameters p_4 and p_5 and the correlation coefficient R^2 for each specimen are shown in Table 3. Theoretically, the 3D morphology parameters affect the relationship between the mechanical aperture and the normal stress. Thus, the 3D morphology parameters should have effect on the fitting parameters p_4 and p_5 in equation (14) too. The relationship between the fitting parameter p_4 and the average peak density $(S_{pd})_{ave}$ and that between the parameter p_5 and $(S_{pd})_{ave}$ are illustrated in Figure 7, respectively. It can be seen from Figure 7 that both p_4 and p_5 are exponentially related to $(S_{pd})_{ave}$ with the correlation coefficients R^2 of 0.97 and 0.98, respectively, and p_4 increases with the increase of $(S_{pd})_{ave}$ while p_5 decreases with the increase of $(S_{pd})_{ave}$. Correspondingly, the average peak density $(S_{pd})_{ave}$ of the fracture surfaces influences the size of the mechanical aperture directly. The greater the average peak density is, the smaller the mechanical aperture is under the same normal stress.

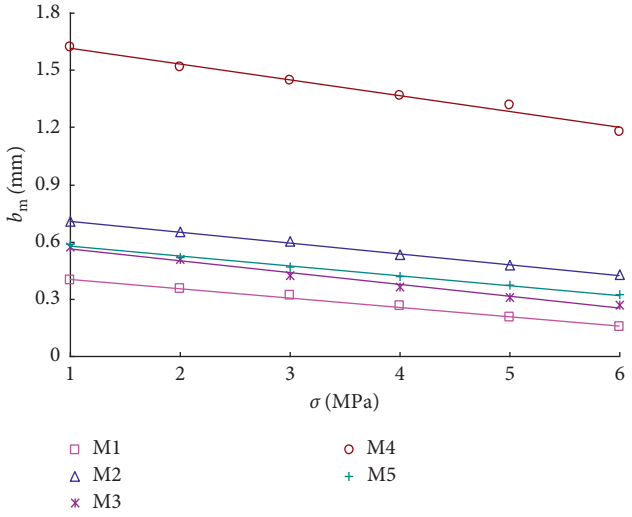

Figure 6: Relationships between the mechanical aperture and the normal stress.

Substituting the relationship between p_4 and $(S_{pd})_{ave}$ and that between p_5 and $(S_{pd})_{ave}$ in Figure 8 into equation (14), the following equation can be obtained:

$$b_m = -\left(0.026 + 2.73e^{-13.54\left(S_{pd}\right)_{ave}}\right)\sigma + 7.26 \times 10^4 e^{-38.27\left(S_{pd}\right)_{ave}} + 0.42. \tag{15}$$

If equation (15) is substituted into equation (13), the following equation is obtained:

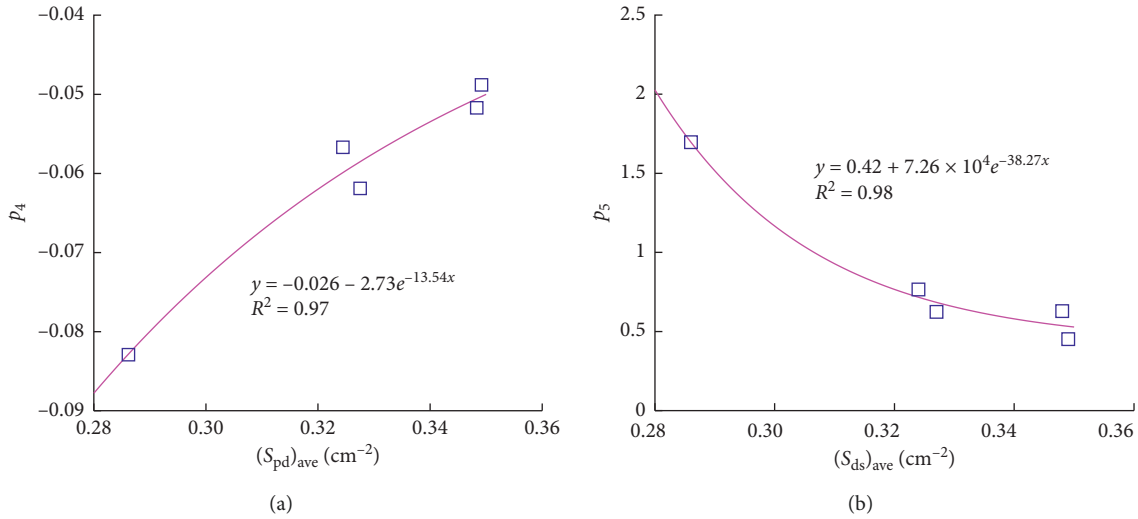

Figure 7: Relationship between fitting parameters p_4, p_5, and $(S_{pd})_{ave}$. (a) p_4 vs $(S_{pd})_{ave}$; (b) p_5 vs $(S_{pd})_{ave}$.

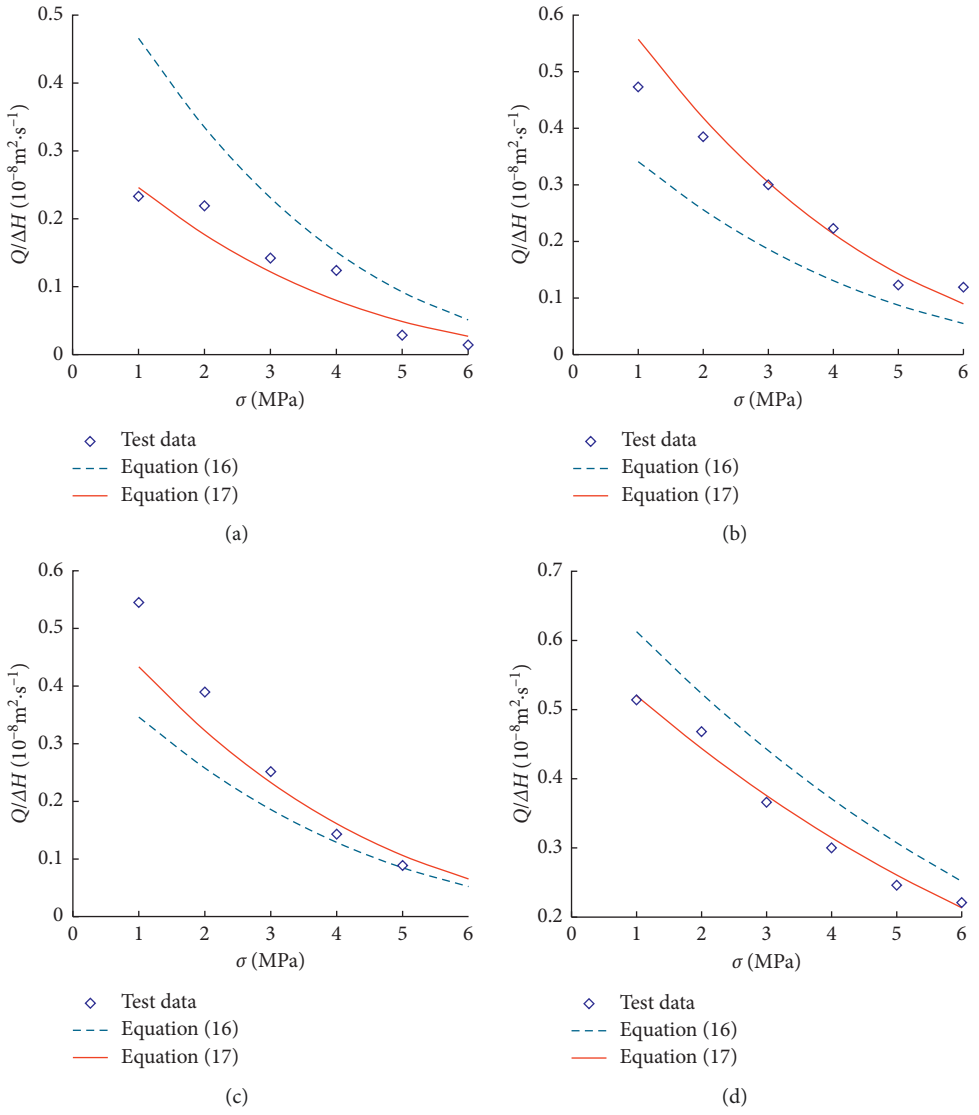

Figure 8: Continued.

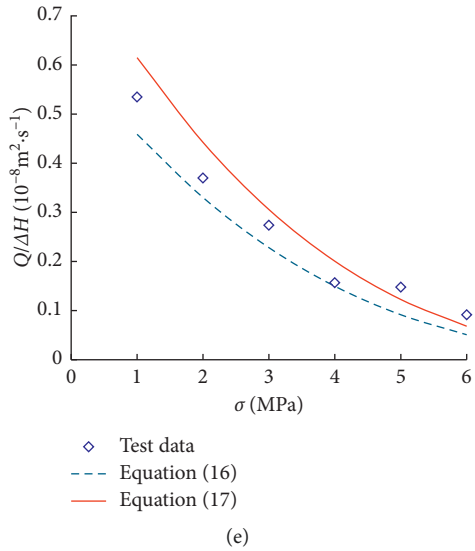

(e)

Figure 8: Comparison of the calculated value by using equation (16) and test data. (a) M1. (b) M2. (c) M3. (d) M4. (e) M5.

$$\frac{Q}{\Delta H} = C \times 10^8 \left(S_{pd}\right)_{ave}^{16.83} \cdot \left[-\left(0.026 + 2.73e^{-13.54\left(S_{pd}\right)_{ave}}\right)\sigma + 7.26 \times 10^4 e^{-38.27\left(S_{pd}\right)_{ave}} + 0.42\right]^3. \quad (16)$$

In equation (16), $(S_{pd})_{ave}$ can be obtained by adopting 3D laser scanner and Rock Joint Morphology Test Software and all other parameters can be obtained easily, too, during the fracture seepage test. Thus, equation (16) provides an important new relationship between the flow rate and the normal stress taking the influence of the fracture roughness into account through incorporating the 3D morphology parameter S_{pd}.

3.6. The Amendment of Equation (16). Figure 8 depicts the relationships between the flow rate per head and the normal stress obtained both experimentally from the fracture seepage tests and theoretically according to equation (16). There exists obvious deviation between the theoretical prediction using equation (16) and the experimental data from the fracture seepage tests. Specially, the theoretical prediction using equation (16) is larger than the experimental data for specimens M1 and M4 and is lower than the experimental data for other specimens, which may be because equation (16) contains total errors of equations (10)~(16). From Table 1, we can see that $(S_{pd})_{max}$ of specimens M1 and M4 are also larger than other specimens so that the deviation between the theoretical prediction using equation (16) and the experimental data may has some relation with $(S_{pd})_{max}$. Thus, an amendment coefficient k is introduced, which is the average ratio between the flow rates per head obtained experimentally from the fracture seepage test and theoretically using equation (16). The relationship between k and the maximum peak density of the fracture surface $(S_{pd})_{max}$ for the five specimens is shown in Figure 9. It can be seen from Figure 9 that the amendment coefficient

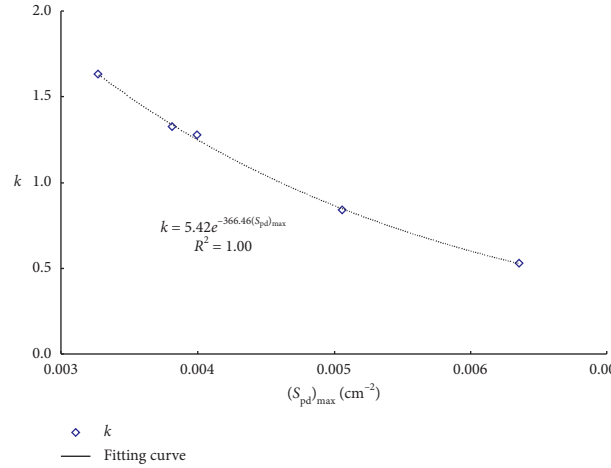

Figure 9: Relationship between k and $(S_{pd})_{max}$.

k has an exponential relationship with $(S_{pd})_{max}$, and the fitting correlation coefficient R^2 is more than 0.99.

After introducing the amendment coefficient, equation (16) becomes

$$\frac{Q}{\Delta H} = 5.42e^{-3.66\left(S_{pd}\right)_{max}}\left(S_{pd}\right)_{ave}^{16.83} C \times 10^8 \cdot \left[0.42 + 7.26 \times 10^4 e^{-38.27\left(S_{pd}\right)_{ave}} - \left(0.026 + 2.73e^{-13.54\left(S_{pd}\right)_{ave}}\right)\sigma_n\right]^3. \quad (17)$$

The relationships between the flow rate per head and the normal stress obtained theoretically according to equation (17) are also illustrated in Figure 8. It can be seen from Figure 8 that after including a 3D morphology parameter, i.e., the peak density, the cubic model in equation (17) predicts the relationship between the flow rate per head and the normal stress in the rock fracture seepage test well. Therefore, equation (17) may be used in numerical simulation or theoretical prediction on the flow rate per head in

the rock fracture seepage test under different normal stresses with the peak density taken into account.

4. Conclusions

(1) There is a linear relationship between the equivalent hydraulic aperture and the fracture closure during the rough rock fracture seepage tests under various normal stresses. The equivalent hydraulic aperture decreases with the increase of the fracture closure. The total normal closure can be set as the maximum mechanical aperture, and then the mechanical aperture under different normal stresses can be calculated by subtracting the normal closure from the maximum mechanical aperture.

(2) There is a power relationship between the flow rate per head and the mechanical aperture, and the index n is close to 3. Thus, the relationship between the flow rate per head and the mechanical aperture meets approximately the cubic model. Since the mechanical aperture cannot be measured easily from the rock fracture seepage test, a correction coefficient ξ is introduced to relate the mechanical aperture to the average peak density $(S_{pd})_{ave}$, which is a 3D morphology parameter to be measured easily.

(3) The mechanical aperture has a linear relationship with the normal stress during the rough rock fracture seepage tests, and the mechanical aperture decreases with the increase of the normal stress.

(4) Equation (13) is a modified cubic law containing the 3D morphology parameter $(S_{pd})_{ave}$ of rock fracture, which can describe the influence of rock fracture roughness on the cubic relationship between the flow rate per head and the mechanical aperture. Equation (17) is suitable to predict the relationship between the flow rate per head and the normal stress of rock fracture after including a 3D morphology parameter $(S_{pd})_{max}$.

Data Availability

The research data used to support the findings of this study are included within the article. Request for more details should be made to the corresponding author.

Conflicts of Interest

The authors declare no conflicts of interest.

Acknowledgments

This research was funded by the China National Natural Science Foundation (grant no. 51109076).

References

[1] G. De Marsily, *Quantitative Hydrogeology: Groundwater Hydrology for engineers*, Academic Press, Orlando, FL, USA, 1986.

[2] G. M. Lomize, *Flow in Fractured Rocks*, Gosenergoizdat, Moscow, Russia, in Russian, 1951.

[3] E. S. Romm, *Flow Characteristics of Fractured Rocks*, Nedra, Moscow, Russia, 1966.

[4] C. A. Louis, "Study of groundwater flow in jointed rock and its influence on the stability of rock mass," Imperial College Rock Mechanics Report 10, Imperial College of Science and Technology, London, UK, 1969.

[5] D. Elsworth and T. W. Doe, "Application of non-linear flow laws in determining rock fissure geometry from single borehole pumping tests," *International Journal of Rock Mechanics & Mining Science & Geomechanics Abstracts*, vol. 23, no. 3, pp. 245–254, 1986.

[6] J. C. Jaeger and N. Cook, *Fundamentals of Rock Mechanics*, Publication of Chapman & Hall, London, UK, 2nd edition, 1976.

[7] K. K. Singh, D. N. Singh, and P. G. Ranjith, "Laboratory simulation of flow through single fractured granite," *Rock Mechanics and Rock Engineering*, vol. 48, no. 3, pp. 987–1000, 2015.

[8] J. S. Konzuk and B. H. Kueper, "Evaluation of cubic law based models describing single-phase flow through a rough-walled fracture," *Water Resources Research*, vol. 40, no. 2, pp. 389–391, 2004.

[9] K. G. Raven and J. E. Gale, "Water flow in a natural rock fracture as a function of stress and sample size," *International Journal of Rock Mechanics & Mining Sciences & Geomechanics Abstracts*, vol. 22, no. 85, pp. 251–261, 1985.

[10] P. A. Witherspoon, J. S. Y. Wang, K. Iwai, and J. E. Gale, "Validity of Cubic Law for fluid flow in a deformable rock fracture," *Water Resources Research*, vol. 16, no. 6, pp. 1016–1024, 1980.

[11] P. A. Witherspoon, "Effect of size on fluid movement in rock fractures," *Geophysical Research Letters*, vol. 8, no. 7, pp. 659–661, 1981.

[12] N. Barton and V. Choubey, "The shear strength of rock joints in theory and practice," *Rock Mechanics Felsmechanik Mecanique des Roches*, vol. 10, no. 1-2, pp. 1–54, 1977.

[13] C. E. Neuzil, "Groundwater flow in low-permeability environments," *Water Resources Research*, vol. 22, no. 8, pp. 1163–1195, 1986.

[14] C. K. Park and P. S. Hahn, "Effects of aperture density distribution on the flow through a rock fracture with line-source and line-collection," *Nuclear Engineering & Technology*, vol. 30, pp. 485–495, 1998.

[15] K. Iwai, *Fundamental Studies of Fluid Flow through a Single fracture*, University of California, Oakland, CA, USA, 1976.

[16] C. Zhou and W. A. Xiong, "Generalized cubic law for percolation in rock joints," *Rock and Soil Mechanics*, vol. 17, no. 4, pp. 1–7, 1996.

[17] J. Zhao, "Joint surface matching and shear strength part B: JRC-JMC shear strength criterion," *International Journal of Rock Mechanics and Mining Sciences*, vol. 34, no. 2, pp. 179–185, 1997.

[18] Y. W. Tsang and C. F. Tsang, "Channel model of flow through fractured media," *Water Resources Research*, vol. 23, no. 3, pp. 467–479, 1987.

[19] M. Luis, G. Björn, and N. Ivars, "Solute transport in fractured media—the important mechanisms for performance assessment," *Journal of Contaminant Hydrology*, vol. 25, no. 3-4, pp. 283–298, 1997.

[20] S. R. Brown, H. W. Stockman, and S. J. Reeves, "Applicability of the Reynolds equation for modeling fluid flow between rough surfaces," *Geophysical Research Letters*, vol. 22, no. 18, pp. 2537–2540, 1995.

[21] Z. Zhang and J. Nemcik, "Friction factor of water flow through rough rock fractures," *Rock Mechanics and Rock Engineering*, vol. 46, no. 5, pp. 1125–1134, 2013.

[22] R. W. Fox, A. T. Mcdonald, and P. J. Pritchard, *Introduction to Fluid Mechanics*, John Wiley & Sons, Hoboken, NJ, USA, 6th edition, 2004.